Characteristics of Ultra-Wideband Bandpass YBCO Filter With Impendence Stub

Li-Min Wang, Wi-Chun Lin, Min-Long Chang, Chiuan-Yu Shiau, and Chun-Te Wu

***Abstract*—A compact ultra-wideband (UWB) bandpass filter (BPF) is presented for applications to short-range and high-speed wireless communication. Superconducting $YBa_2Cu_3O_y$ (YBCO) stepped impedance resonators and coupled-line sections as inverter circuits are designed to form the basic filter structure. In the filter design, connected high-low stepped impedance microstrip lines construct the resonators, and open-stub lines are utilized to add return-loss poles in the pass-band and create transmission zeros in the lower/upper stop-band region. Simulation results show that the passband from 3.0 GHz to 8.6 GHz has a 3-dB fractional bandwidth of 99 percent, computed insertion losses better than 0.03 dB, and return losses greater than 15 dB. Rejection levels in the upper/lower stop-bands are better than 20 dB. For fabrication, high-T_c superconducting (HTS) YBCO films were deposited on double-side-polished 0.5-mm-thick MgO (100) substrates by a radio-frequency sputtering system. The filter was made out of patterned double-sided deposited YBCO films integrated with a gold-coated housing. The realized HTS UWB BPF shows a wide passband within 2.9–8.3 GHz with a maximum insertion loss of 0.88 dB. The measured results show good HTS UWB BPF performance. Moreover, the temperature-dependent frequency responses and the insertion loss can be described by the modified two-fluid-model-based formulas, indicating that the frequency shift and the increase in insertion loss for HTS BPF are both dominated by the temperature dependence of the magnetic penetration depth.**

***Index Terms*—Bandpass filter (BPF), high-temperature superconductors, multiple-mode resonator (MMR), stepped impedance resonator (SIR), ultra-wideband (UWB).**

I. Introduction

ULTRA-WIDEBAND (UWB) technologies have attracted much attention in recent years due to their potential applications to modern transmission systems, such as local area networks, through-wall imaging, vehicular radar systems, position location and tracking, as well as indoor and hand-held UWB systems [1]. In particular, since the Federal Communications Commission (FCC) released the unlicensed use of the UWB (3.1–10.6 GHz), there has been much research on UWB components and devices, which have the advantages of low cost, high-speed transmission, and low power consumption [2]–[13]. One of the key devices in almost any communication system is the bandpass filter (BPF), which is required to have low insertion loss over the pass band and to exhibit very good selectivity near the passband skirts. However, designing a good-performance UWB BPF is definitely a challenge due to the requirement of large fractional bandwidth, which accompanies theoretically unexpected spurious resonances and uncontrollable nonlinear frequency dispersion. One should note that the microwave filter theory was developed from the assumption of a narrow fractional bandwidth. Thus, different realizations of UWB BPFs have been reported, such as microstrip-ring-type filters [2], [3], BPFs using multilayer liquid crystal polymer technology [4], [5], BPFs with stepped-impedance multiple-mode resonator (MMR) [6]–[11], BPFs with composite series and shunt stubs [12], and packaged BPFs with combination of MMR and ring resonators [13]. On the other hand, it is well known that a high-temperature superconducting (HTS) microwave device has lower loss and better performance than a normal-conducting one. However, only few attempts have so far been devoted to construction of UWB BPFs using HTS materials [14]. Furthermore, with regard to the cryogenic environment for HTS filters, developing HTS filters to a minimum size is important for reducing the cooling space and power consumption of the refrigeration system. In this article, a UWB HTS BPF constructed using stepped-impedance resonators (SIRs) with tight coupling and an impedance stub is proposed. The HTS filter is designed within a 15×10-mm^2 area using double-sided deposited $YBa_2Cu_3O_y$ (YBCO) films grown on MgO substrates. The temperature-dependent microwave properties of our HTS BPFs are also discussed.

II. Filter Design and Experiments

Figs. 1(a) and 1(b) show the geometries of the designed UWB BPF without and with an impedance stub, respectively. The layouts are similar to those introduced in [8]. Theoretical analyses for this kind of UWB BPFs with MMRs have been proposed in [7]–[9]. Basically, the layout includes the centered transmission-line resonator with impedance steps and two folded sections of parallel-coupled microstrip lines. The two parallel-coupled microstrip line sections create two in-band reflection zeros and a broadband BPF can be created with a single-line resonator. The lengths of parallel-coupled microstrip line sections are a quarter-wavelength at center frequency with very tight coupling to create a broad pass-band. The centered transmission line is half a wavelength long with low characteristic impedances. In Fig. 1(b), an additional open-ended stub is added to the centered transmission line to create a strong reflection zero

Manuscript received August 03, 2010; accepted November 01, 2010. Date of publication December 10, 2010; date of current version May 27, 2011. This work was supported by the National Science Council of the Republic of China under Grant NSC 98-2112-M-212-001-MY3.

L.-M. Wang is with the Graduate Institute of Applied Physics, National Taiwan University, Taipei 10617, Taiwan (e-mail: liminwang@ntu.edu.tw).

W.-C. Lin, M.-L. Chang, C.-Y. Shiau, and C.-T. Wu are with the Department of Electrical Engineering, Da-Yeh University, Chang-Hwa 515, Taiwan.

Color versions of one or more of the figures in this paper are available online at http://ieeexplore.ieee.org.

Digital Object Identifier 10.1109/TASC.2010.2091231

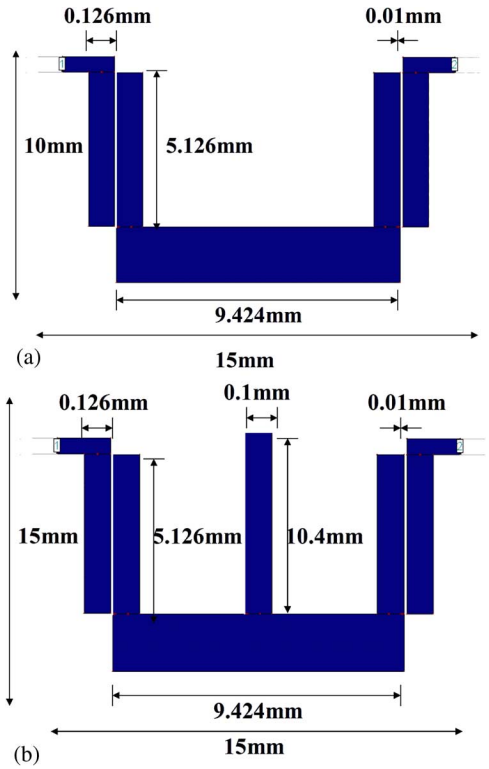

Fig. 1. Geometries of the proposed UWB BPFs (a) without and (b) with an open-ended stub.

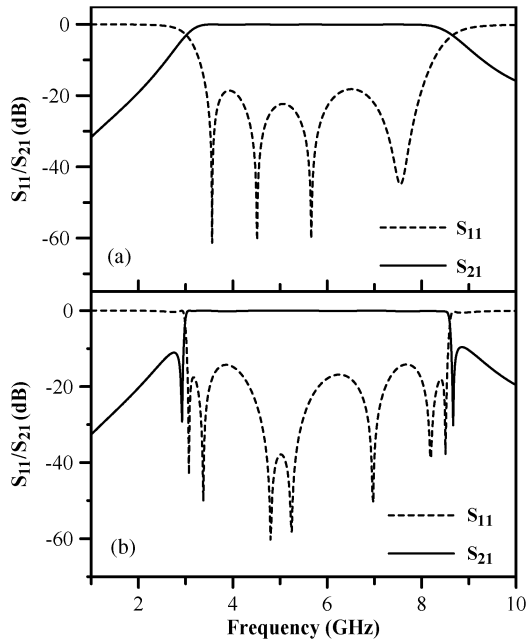

Fig. 2. Simulation results for the proposed UWB BPFs (a) without and (b) with an open-ended stub.

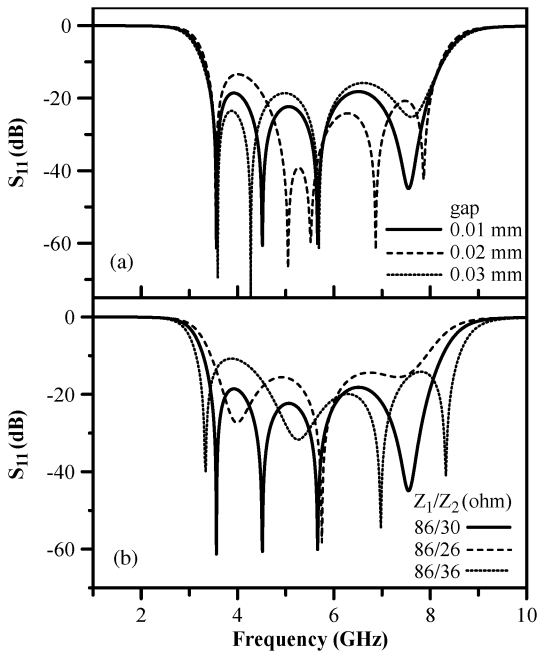

Fig. 3. Some simulated S_{11} frequency responses for (a) various gap distances and (b) SIR impedances.

in passband and a sharp transmission zero at the band edge. The stub has resonance length close to a quarter-wavelength at the upper passband frequency as well as high impedance to reduce the impact on the passband. Figs. 2(a) and 2(b) respectively show the frequency responses S_{11} and S_{21} of the simulation results for the designs shown in Figs. 1(a) and 1(b) using the IE3D Software. The designed filter as shown in Fig. 2(a) has the center frequency f_c at 5.83 GHz with a bandwidth of 5.62 GHz (3.02–8.64 GHz), corresponding to a fractional bandwidth of 99 percent. Comparing with the results shown in Fig. 2(a) shows that a pair of reflection zeros and sharp transmission zeros at the band edges can be obtained for the design with an additional open-ended stub. The designed filter with an additional open-ended stub as shown in Fig. 2(b) has the center frequency of f_c at 5.79 GHz with transmission zeros near the passband edges. Additionally, the simulation results show that the passband from 2.99 GHz to 8.59 GHz has a 3-dB fractional bandwidth of 97 percent, computed insertion losses better than 0.15 dB and return losses greater than 15 dB. Rejection levels in the upper/lower stop-bands are better than 20 dB, showing a good filter design. Moreover, the characteristic impedance and gap distance in the parallel-coupled microstrip line sections have to be adjusted toward tight coupling, and the characteristic stepped impedances, Z_1 and Z_2 respectively for the coupled microstrip line and middle transmission line, to obtain an optimal performance. Figs. 3(a) and 3(b) show some typical simulated S_{11} responses for various gap distances and the SIR impedances, respectively. As can be seen, the frequency response S_{11} is very sensitive to the gap distance and the SIRs of the centered transmission-line resonator. This poses challenges for the fabrication of realized filters. Via fine tuning, a gap distance of 0.01 mm, $Z_1 = 86\ \Omega$, and $Z_2 = 30\ \Omega$ are chosen as the optimal filter designs.

In experiments, HTS 500-nm-thick YBCO films were deposited onto a double-side-polished $15\times10-\mathrm{mm}^2$ and 0.5-mm-thick MgO substrates using a radio-frequency sputtering system and were patterned with etching to form the designed structure. The fabrication and package processes were similar to those

reported previously [15]. An HP 8714ES vector network analyser (VNA) with a pair of cryogenic cables (which can be operated within 150°C and −269°C) was employed to measure the reflection and transmission coefficients. For measurement, one end of the cryogenic cable was connected to the VNA input/output port, and the other was connected to the input/output SMA connectors of the packaged HTS filter. The filter was then put into a cryogenic vacuum system to do the measurements. In addition, the frequency responses for a 50-Ω superconducting transmission line shorting the SMA connectors were also measured to calibrate the signal loss occurring at the interfaces between the superconducting microstripline and SMA connecters.

III. Results and Discussion

Figs. 4(a) and 4(b) show the frequency responses of the experimental data measured at 77 K for the designs shown in Figs. 1(a) and 1(b), respectively. The simulation results are also shown for comparison. In Fig. 4(a), the measured frequency responses show that the passband from 2.88 GHz to 8.30 GHz has a fractional bandwidth of 99 percent and insertion losses better than 2.42 dB for the realized UWB BPF without an open stub. On the other hand, the frequency responses for the realized UWB BPF with an open stub show that the passband from 2.90 GHz to 8.40 GHz has a fractional bandwidth of 97 percent and insertion losses better than 0.88 dB, as shown in Fig. 4(b). The realized UWB BPF with an open stub shows better performance and has transmission zeros near the passband edges to improve the passband skirts. Additionally, the measurement results for the two fabricated filters reveal shifting of passbands to a lower frequency region. The frequency deviation between the EM simulations and experimental results may be attributed to variations in resonator size introduced in the fabrication process. Deviations of several μm from the designed resonator dimensions due to lithography and etching processes were observed in the HTS filter. This YBCO BPF, realized using MMRs with an open stub, shows a low insertion loss with UWB behavior within the frequency region of 2.90–8.40 GHz. To the best of the authors' knowledge, this has not been reported in the literature. Hereafter, we will focus on the temperature-dependent microwave properties of the proposed UWB HTS BPF.

To further clarify the microwave properties of HTS filters, it is essential to understand the temperature dependence of the frequency responses. Figs. 5(a) and 5(b) show the temperature dependences of the experimental center frequency f_c and the maximum insertion loss IL_{max} for the filter with an open stub, respectively. As can be seen, f_c shifts to lower frequencies and shows a rapid drop as the temperature approaches T_c. Also shown in Fig. 5(a) is the calculated center frequency as denoted by the fitting curve. The center frequency f_c can be calculated by the following equation [16],

$$f_c = C\left[1 + 2(\lambda_p/h)coth(d/\lambda_p)\right]^{-0.5}, \quad (1)$$

where C is a fitting parameter, λ_p is the magnetic penetration depth, d is the thickness of YBCO film, and h is the thickness of substrate. Here $d = 500$ nm and $h = 0.5$ mm are used. The temperature dependence of λ_p was reported by Rauch *et al.* [17], which is given by

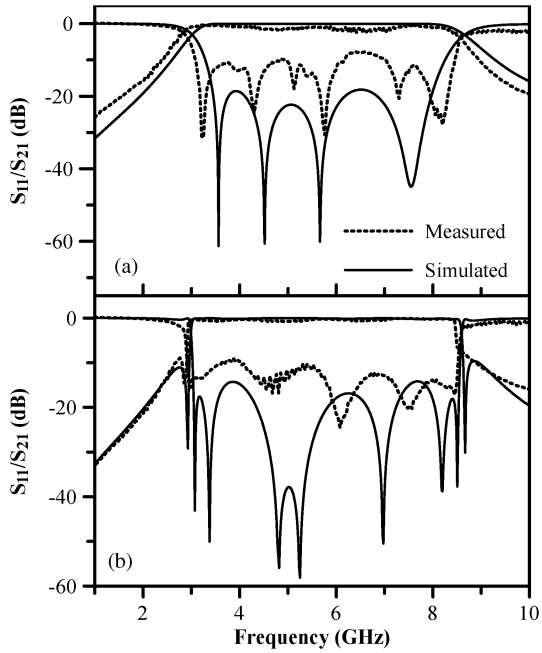

Fig. 4. Frequency responses of the simulation results and the experimental data measured at 77 K for the proposed UWB BPFs (a) without and (b) with an open-ended stub.

$$\lambda_p(T) = \lambda_0\left[1 - 0.1(T/T_c) - 0.9(T/T_c)^2\right]^{-0.5}, \quad (2)$$

where λ_0 is the magnetic penetration depth at zero temperature. In the simulation using formulas (1) and (2), our best fit for f_c is obtained with $\lambda_0 = 1011$ nm, $C = 5.66$ GHz, and $T_c = 81.3$ K, as demonstrated by the curve shown in Fig. 5(a). As seen, the measured temperature-dependent f_c can be described by formulas (1) and (2), indicating that the frequency shift in HTS filter is dominated by the temperature dependence of the magnetic penetration depth. On the other hand, as seen in Fig. 5(b), IL_{max} increases with increase in temperature. The insertion loss increases up to 4.7 dB at 81 K. Such increase can be attributed to the increased surface resistance of YBCO films as the temperature approaches the critical value T_c. Basically, the insertion loss is proportional to the surface resistance R_s. R_s, derived from the two-fluid model, can be described by the following formula:

$$R_s = 2\pi^2\sigma_N f^2\mu_0^2(\lambda_p)^3, \quad (3)$$

where σ_N is the normal-state conductivity of the superconductors. Using formulas (2) and (3), and $IL_{max} \propto R_s$, we can well describe the temperature dependence of IL_{max} with a prefactor of 0.62 dB, as shown in Fig. 5(b). The large λ_0 value derived for YBCO still remains to be further clarified within the theoretical work for UWB BPFs.

IV. Conclusion

UWB HTS BPFs were proposed and fabricated for applications on short-range and high-speed wireless communication. The filters designed using MMRs show UWB-response characteristics. The configuration with an extra open-ended stub added

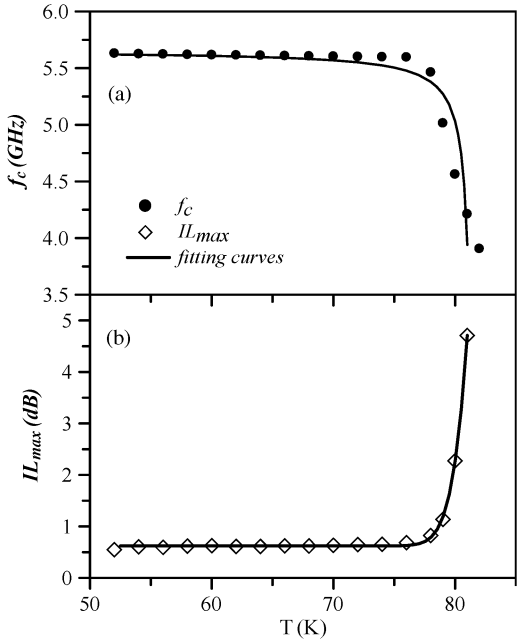

Fig. 5. Temperature dependences of (a) the experimental center frequency and (b) the maximum insertion loss for the UWB BPF with an open-ended stub.

to the centered transmission line makes the rejection slope sharp by producing a single pair of transmission zeros near the passband edge. The realized UWB HTS BPF with an open stub shows a UWB passband of 2.90–8.40 GHz with a maximum insertion loss of 0.88 dB. The measured results show good UWB HTS BPF performance. Moreover, both the center frequency and insertion loss measured can be described by the presented formulas, indicating that the frequency shift and the increase in insertion loss for the HTS filter are due to the temperature dependence of the magnetic penetration depth.

REFERENCES

[1] Federal Communications Commission, Revision of Part 15 of the Commission's Rules Regarding Ultra-Wideband Transmission Systems, ET-Docket 98-153, FCC02-48, Apr. 2002, Tech. Rep..

[2] H. Ishida and K. Araki, "Design and analysis of UWB bandpass filter," in *Proc. IEEE Wireless Comm. Tech. Top. Conf.*, Oct. 2003, pp. 457–458.

[3] C.-L. Hsu, F.-C. Hsu, and J.-T. Kuo, "Microstrip bandpass filters for ultra-wideband (UWB) wireless communications," *IEEE MTT-S Lnt. Microw. Symp.*, pp. 679–682, Jun. 2005.

[4] Z.-C. Hao and J.-S. Hong, "Compact wide stopband ultra wideband bandpass filter using multilayer liquid crystal polymer technology," *IEEE Microw. Wireless Compon. Lett.*, vol. 19, no. 5, pp. 290–292, May 2009.

[5] Z. C. Hao and J. S. Hong, "Quasi-ellipitic UWB bandpass filter using multilayer liquid crystal polymer technology," *IEEE Microwave and Wireless Components Letters*, vol. 20, no. 4, pp. 202–204, Apr. 2010.

[6] L. Zhu, S. Yun, and W. Menzel, "Ultra-wideband (UWB) bandpass filters using multiple-mode resonator," *IEEE Microwave and Wireless Components Letters*, vol. 15, no. 11, pp. 796–798, Nov. 2005.

[7] P. Cai, Z. Ma, X. Guan, Y. Kobayashi, T. Anada, and G. Hagiwara, "Synthesis and realization of novel ultra-wideband bandpass filters using 3/4 wavelength parallel-coupled line resonators," in *Proc. of Asia-Pacific Microwave Conference 2006*, Yokohama, Japan, Dec. 2006, vol. 1, pp. 159–162.

[8] M. Mokhataari, J. Bornemann, and S. Amari, "Compact planar ultra-wide pass-band filters with source-load coupling and impedence stubs," in *Proc. of Asia-Pacific Microwave Conference 2006*, Yokohama, Japan, Dec. 2006, vol. 1, pp. 155–158.

[9] Y.-C. Chiou, J. T. Kuo, and E. Cheng, "Broadband quasi-chebyshev bandpass filters with multimode stepped impedance resonators (SIRs)," *IEEE Trans. Microwave Theory and Techniques*, vol. 54, no. 8, pp. 3352–3356, Aug. 2006.

[10] C. Y. Hsu, L. K. Yeh, C. Y. Chen, and H. R. Chuang, "A 3–10 GHz ultra-wideband bandpass filter with 5–6 GHz rejection band," in *Proc. of Asia-Pacific Microwave Conference 2007*, Bangkok, Thailand, Dec. 2007, vol. 1, pp. 1–4.

[11] P. Cai, Z. Ma, X. Guan, X. Yang, Y. Kobayashi, T. Anada, and G. Hagiwara, "A compact UWB bandpass filter using two-section open-circuited stubs to realize transmission zeros," in *Proc. of Asia-Pacific Microwave Conference 2005*, Suzhou, Jiangsu Sheng, China, Dec. 2005, vol. 5, pp. 3356–3359.

[12] R. Li, S. Sun, and L. Zhu, "Synthesis design of ultra-wideband bandpass filters with composite series and shunt stubs," *IEEE Trans. Microw. Theory Tech.*, vol. 57, no. 3, pp. 682–692, Mar. 2005.

[13] L. Han, K. Wu, and X. Zhang, "Development of packaged ultra-wideband bandpass filters," *IEEE Trans. Microwave Theory and Techniques*, vol. 58, no. 1, pp. 220–227, Jan. 2010.

[14] W. Chen, X. Guo, B. Cao, X. Zhang, B. Wei, Y. Zhang, and X. Lu, "A superconducting microstrip ultra-wideband (UWB) bandpass filter at VHF-band," *IEEE Microwave and Wireless Components Letters*, vol. 19, no. 10, pp. 635–637, Oct. 2009.

[15] L. M. Wang, C. H. Hsieh, and C. C. Chang, "Cross-coupled narrowband filter for the frequency range of 2.1 GHz using YBCO resonators with artificial magnetic pinning lattices," *IEEE Trans. Appl. Supercond.*, vol. 15, no. 2, pp. 1040–1043, June 2005.

[16] D. Okai, M. Kusunoki, M. Mukaida, and S. Ohshima, "New measurement technique of the surface impedance of superconductors using the probe-coupling type microstripline resonator," in *Proc. of APMC'99*, Raffles, Singapore, Nov. 1999, vol. 3, pp. 880–883.

[17] W. Rauch, E. Gornik, G. Sölkner, A. A. Valenzuela, F. Fox, and H. Behner, "Microwave properties of $YBa_2Cu_3O_{7-x}$ thin films studied with coplanar transmission line resonators," *J. Appl. Phys.*, vol. 73, no. 4, pp. 1866–1872, Feb. 1993.